Evaluation of the soft tissue components of the equine stifle using 3 Tesla magnetic resonance imaging under flexion, extension, and loading

by

Jocelyn Marie Stedman

B.A., Cornell University, 2015
D.V.M., Cornell University College of Veterinary Medicine, 2019

A THESIS

submitted in partial fulfillment of the requirements for the degree

MASTER OF SCIENCE

Department of Clinical Sciences
College of Veterinary Medicine

KANSAS STATE UNIVERSITY
Manhattan, Kansas

2024

Approved by:

Major Professor
John Dylan Lutter, DVM, MS, DACVS-LA

Copyright

Abstract

High field magnetic resonance imaging (MRI) of the equine stifle provides high resolution information about soft tissues that is useful in the diagnosis of stifle lameness. The aim of this prospective anatomic study was to describe the appearance, position, size, and shape of the equine femorotibial ligaments, meniscal ligaments, and menisci using 3 T MRI under extended, extended loaded, and flexed conditions. Additionally, histologic examination of the collateral and cruciate ligaments of a single stifle was performed to compare with MRI images. In extension, mild variations in MRI signal intensity were apparent in the cruciate ligaments and the cranial had two distinct longitudinal regions indicating two ligament bundles. Flexion had minor effects on cruciate ligament signal intensity and altered the tibial angles of attachment. Histology indicated that both cruciate ligaments were comprised of two fiber bundles. The collateral ligaments were the same low-signal intensity. The medial collateral ligament had a smaller cross-sectional area than the lateral, and flexion increased the length of the medial collateral ligament and the cross-sectional area of the lateral. Low loads in extension did not affect the MRI appearance of stifle soft tissues. Flexion of the stifle impacted cruciate ligament insertion angles and the size and shape of the collateral ligaments. This study provides support for the use of MRI to understand the anatomy and function of stifle ligaments.

Table of Contents

List of Figures

List of Tables

Acknowledgements

I would like to thank my major professor, Dr. Dylan Lutter, along with the other members of my committee, Dr. Clay Hallman and Dr. Elizabeth Santschi, for their support and assistance in developing this thesis. Additionally, I would like to express my appreciation to Nicholas Hemphill for acquisition of the MRI images, Maria Granello for assistance in preparation of the cadaver limbs, Sheila Laverty and Hélène Richard for histologic processing and interpretation, and Robert Larson and Eduarda Bortoluzzi for assistance with statistical analysis.

Chapter 1 - Introduction

The equine stifle is the largest most complex joint in the horse and a common area of injury resulting in lameness and loss of performance (1-3). Soft tissue injuries are being increasingly recognized as a cause of these stifle injuries (3). A variety of imaging modalities have been described to diagnose and characterize lesions of the stifle but no technique currently in clinical use allows full evaluation of the osseous and soft tissue structures of the joint. Radiography, ultrasonography, arthroscopy, and computed tomography (CT) have all been used to evaluate the equine stifle, but each have limitations, especially in soft tissue imaging, due to inherent technology restrictions and the anatomy of the stifle (4-10). Specifically, the location of multiple soft tissue structures including the cruciate ligaments, meniscotibial ligaments, meniscofemoral ligament, and the axial and caudal aspects of the menisci makes full evaluation difficult (4,6,11).

Magnetic resonance imaging (MRI) is considered the gold standard for imaging soft tissue structures and in humans is the preferred imaging modality for evaluation of the knee (12,13). At this time, the clinical use of MRI for the diagnosis of stifle injuries in the horse is limited by magnet bore diameter (14). MRI has been used in cadaveric adult equine stifles to define normal and abnormal structures within the equine stifle, which will allow for more rapid clinical adoption of stifle MRIs when this technology becomes available (15,16).

Human cruciate ligaments have a heterogenous fiber alignment, composition and attachment, and fiber alignment changes with joint motion (17). Specifically, the human anterior cruciate ligament consists of an anteromedial and posterolateral bundle, while the posterior cruciate ligament consists of an anterolateral and posteromedial bundle, with the bundles named for their tibial insertion sites (18,19). This anatomy and the impact of load and flexion on the soft

tissue components in the horse has not been investigated. Imaging of equine cadaver specimens in extended (EXT), extended loaded (EXTload) and flexed (FLEX) conditions would increase understanding of joint kinematics and may generate hypotheses for the etiopathogenesis of injuries such as meniscal tears, cruciate ligament injuries, subchondral bone injury, and cartilage damage (20) as has been done using dynamic MRI in humans (21). Additionally, the histology of the equine cruciate ligaments has not been described and correlation of MRI and histologic findings would allow for better understanding of the relevance of changes seen on MRI.

The objective of this study was to evaluate the appearance, position, and shape of the cranial and caudal cruciate ligaments, the medial and lateral menisci, and the collateral ligaments of the stifle, using 3T MRI under flexed, extended and loaded conditions. A secondary objective was to examine the histologic structure of the cruciate ligaments of the stifle to demonstrate the presence of two bundles in each respective ligament and to correlate these structures with the MRI appearance of these ligaments.

Chapter 2 - Materials and Methods

This prospective cadaveric anatomic study was approved by the Kansas State University Institutional Animal Care and Use Committee (IACUC-4679). Three left and right stifles were collected from 6 adult horses euthanized at the Kansas State University Veterinary Health Center in 2022 for reasons unrelated to hindlimb lameness.

Limb preparation

Within 12 hours of euthanasia, a stifle from each horse was removed by disarticulating the limb at the coxofemoral joint and transecting the limb at the mid-diaphysis of the tibia. Most muscle tissue was removed but the popliteus muscle was retained to protect the caudal joint soft tissues. The cranial fascia was left intact to protect the distal patellar ligaments and joint capsule (Figure 1). Care was taken to avoid damage to the collateral ligaments. A single, transverse, 12.7 mm bicortical hole was drilled through the distal femur 8 cm proximal to the origin of the collateral ligaments of the stifle. A second parallel bicortical hole was drilled through the proximal tibia 3 cm distal to the insertion of the collateral ligaments of the stifle. A third hole was drilled distal to proximal beginning at the proximal aspect of the middle distal patellar ligament and exiting in the middle of the concave proximal surface of the patella. A unicortical hole was drilled through the dorsal cortex of the femur on midline, 4 cm proximal to the distal femoral drill tract. A 12.7 mm diameter, 12.5 cm long wooden dowel rod was inserted into this hole and hammered firmly into place to serve as an anchor for the patellar cable tie. All limbs were wrapped in saline soaked towels and refrigerated at 4°C overnight prior to imaging.

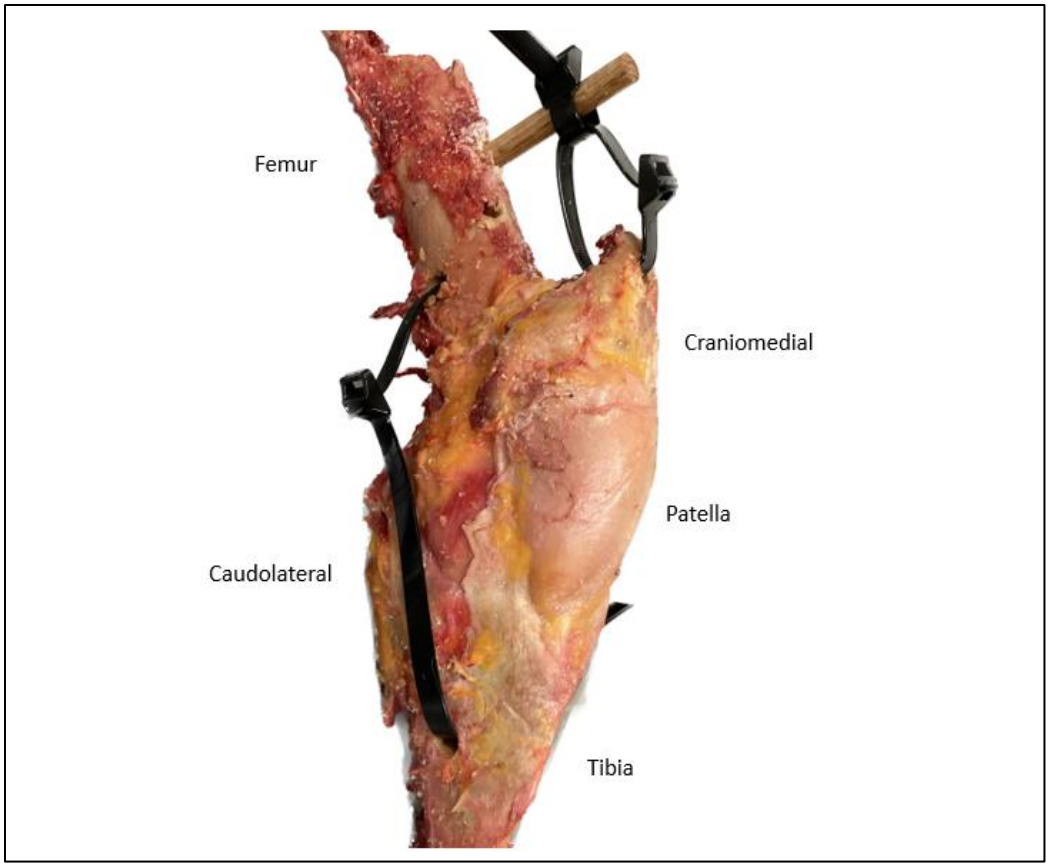

Figure 1: A craniolateral to caudomedial photo of a dissected equine stifle prepared for magnetic resonance imaging in the extended unloaded condition with three drilled holes with attached dowel rod and cable ties.

Magnetic resonance imaging

Magnetic resonance imaging was performed within 36 hours of euthanasia. Seven imaging sequences (Table 1) were performed on each stifle in three different conditions: EXT, EXTLoad, and FLEX. Plastic cable ties were used to achieve these conditions. One cable tie was inserted through the hole in the femur and a second through the hole in the tibia, and the cable ties were connected to provide load across the joint. A third cable tie was looped vertically through the patellar hole and a fourth was looped through that patellar tie and around the wooden dowel rod in the femur to load the patella in tension along the central axis (Figure 1).

For the EXT condition, the stifle was placed in 155° of extension (angles measured by goniometer) and the patellar cable tie tightened to a load of 111N, the minimum load necessary to maintain the patella at the proximal trochlear ridges, maintain extension, provide distal patellar ligament tension, and limit cranial translation of the femur. The cable ties across the joint were not tightened. To achieve EXTLoad, the cable ties across the stifle joint were tightened to 138N, the highest load that could be applied, and the patellar cable tie was unchanged. For the FLEX condition, the stifle was placed in 110° of flexion and new cable ties were placed across the stifle and from the patella to the dowel. The cable ties across the stifle joint were tightened to a load of 89N, the greatest load that could be applied at 110°. The new patellar cable tie was tightened sufficiently to maintain the flexion angle. Cables were tightened using a purpose-built cable tie gun (HellermannTyton, Milwaukee, Wisconsin) with quantitative tension adjustment.

The limb was positioned with the lateral aspect in contact with the scan table. Images were acquired using a large multi-use coil, isocentered within a 3 T magnetic resonance scanner (Vantage Galan 3T, Canon, Oxford, UK) running V5.0 software, with bore diameter 70 cm. The MRI protocol (Table I) was designed to fully evaluate the soft tissue structures of the stifle, including standard Proton Density (PD) Fast Spin Echo (FSE) sequences in the dorsal, sagittal, and transverse planes to allow planning and acquisition of the subsequent novel T2-weighted FSE dorsal oblique, sagittal oblique, and transverse oblique planes based on those previously reported to allow full evaluation of the cranial and caudal cruciate ligaments (15).

Table 1: Magnetic resonance imaging sequence parameters

Sequence	TR	TE	TI	Frequency	Phase	Flip angle	Echo train length	NEX	FOV	Frequency direction	Fat suppressed	Slice thickness	Gap width	Number of slices	Time to run (min)
Sagittal PD FSE	4853.0 - 5005.0	24	n/a	123.20	192	90	5	2	25	S/I	No	2.0000	0	66	7:36
Dorsal PD FSE	8720.0 - 9652.0	18	n/a	123.20	192	90	5	2	26	A/P	No	2.0000	0	82	7:47
Transverse PD FSE	9099.0	24	n/a	123.20	192	90	5	2	18	A/P	No	2.0000	0	120	8:03
Sagittal Oblique T2 FSE	13705.0 - 15663.0	84	n/a	123.20	224	90	15	2	22	A/P	No	2.0000	0	70	4:48
Transverse Oblique T2 FSE	14684.0 - 15663.0	84	n/a	123.20	224	90	15	2	24	A/P	No	2.0000	0	75	5:09
Dorsal Oblique T2 FSE	19774.0	84	n/a	123.20	224	90	15	2	18	A/P	No	2.0000	0	120	6:14
Dorsal Oblique PD FSE	8341.0 - 9099.0	24	n/a	123.20	192	90	5	2	18	A/P	No	2.0000	0	120	6:14

Notes: PD, proton density; FSE, fast spin echo; TR, repetition time; TE, echo time; TI, inversion time; NEX, number of excitations; FOV, field of view

Magnetic resonance image interpretation

Each MRI sequence and imaging plane for the three conditions was assessed by one of the authors (JMS) and then independently reviewed by a board-certified radiologist (CH) and a board-certified equine surgeon with extensive MRI experience (JDL) using standard image processing software (Philips Vue PACS, Rochester, NY, USA). In any areas of disagreement, the images were reviewed by the three assessors together and a consensus was reached regarding the final assessment. Any abnormalities were noted. The appearance of the caudal and cranial cruciate ligaments, the medial and lateral collateral ligaments, the medial and lateral menisci, the distal patellar ligaments and the meniscotibial and meniscofemoral ligaments was thoroughly described with a focus on signal intensity, shape, and fiber pattern.

Measurements were made of the cruciate and collateral ligaments and the menisci under each condition. The length of the cranial cruciate ligament was measured on the T2 FSE dorsal oblique sequences using the slice where the ligament was best visualized in its longitudinal axis. The cross-sectional area (CSA) of the cranial cruciate ligament was measured at the midpoint of its length on the T2 FSE transverse oblique sequences and repeated on the caudal cruciate ligament with the length measured on the T2 FSE transverse oblique sequences and the CSA measured on the T2 FSE dorsal oblique sequences. The tibial angle of insertion of the cruciate ligaments was measured on the T2 FSE sagittal oblique sequences by measuring the angle between the proximal edge of each ligament and the tibial plateau. The length of the medial and lateral collateral ligaments was measured on the dorsal PD FSE sequences from the origin to the insertion using a curvilinear line that traced the abaxial profile of each ligament. The CSA of each collateral ligament was measured at the midpoint. CSA of the cranial and caudal horns and midbody of the medial and lateral menisci were measured on the dorsal PD FSE sequences. All

measurements were made by a single author (JMS) on 3 separate occasions at least 1 week apart in a random order and then averaged.

Histologic evaluation

Histologic evaluation was performed on ligaments from the stifle of a single horse collected during the pilot phase of the study. Following completion of MRI, the specimen was immediately dissected. The medial and lateral collateral ligaments were transected at the origin and insertion and removed intact. The origin and insertion of the cranial and caudal cruciate ligaments were identified and transected to remove the ligaments intact. The cruciate and collateral ligaments were fixed in 10% neutral buffered formalin for 48 hours and then placed in a specimen cup with phosphate buffered formalin for histologic processing. The specimens were shipped to the Comparative Orthopedic Research Laboratory (University of Montreal, Montreal, Canada). Each ligament was photographed prior to sectioning. The central section of the ligament was then cut in both transverse and sagittal planes and embedded in paraffin. Five micrometer sections were cut with a microtome (Thermo Fisher Scientific HM340E Rotary Microtome, Waltham Massachusetts) and mounted on slides. The histological sections were stained with Hematoxylin, Eosin and Phloxin (HEPS) to reveal features of their structure for comparative purposes. All sections were examined with bright field light microscopy and then digitized using a microscope (Leica DM4000B, Deerfield, Illinois) coupled with a camera (Allied Vision Prosilica GT1920C camera, Stadtroda, Germany), and the software Panoptiq (Houston, Texas). The fiber pattern and orientation, arrangement, and cohesiveness, and overall staining intensity were described for each ligament.

Statistical analysis

Data were stored in Microsoft Excel (Microsoft Corp, 2023) and descriptive statistics performed using a commercially available statistical software program (R version 4.2.1, R Core Team, Vienna, Austria). Results were reported as mean +/- standard deviation. The distribution of the data for each variable was checked for normality using a Shapiro-Wilk test. Data that were not normally distributed were log transformed for analysis. The “lmer” function of RStudio was used to build linear mixed models to compare the measurements of the examined structures under the 3 treatments (EXT, EXTLoad, and FLEX), keeping the treatment as a fixed effect and the horse as a random effect to control for lack of independence among horses. The “contrast” function was used to perform pairwise comparisons when necessary. Statistical significance was set at $P < 0.05$.

Chapter 3 - Results

Three left and right stifles were collected from six horses with a mean age of 20.7 +/- 6.3 years. Five were Quarter Horses, one a Missouri Fox Trotter, and 5 were mares and one a gelding (Table 5, Appendix A). All were euthanized for reasons unrelated to hind limb lameness.

MRI description

Cruciate ligaments

The cranial cruciate ligament was best visualized on the T2 weighted FSE dorsal oblique, sagittal oblique, and transverse oblique sequences. In the EXT condition, two distinct regions of signal intensity could be recognized in the ligament, a narrow, more hyperintense medial region, and a more substantial, homogenously hypointense lateral region (Figure 2A). The lateral fibers formed the caudal tibial attachment. The medial region had an intermediate signal intensity on T2 FSE sequences, a high intensity on PD FSE sequences and was heterogenous in appearance. The medial fibers formed the cranial tibial attachment. The medial region appeared longer than the lateral region due to its more caudal femoral origin and more cranial tibial insertion. The cranial cruciate ligament shape was circular at its origin, ovoid centrally and a broad oval at the tibial insertion. A thin rim of low signal intensity surrounded the mid to distal portion of the cranial cruciate ligament on the T2 FSE transverse oblique (Figure 2B).

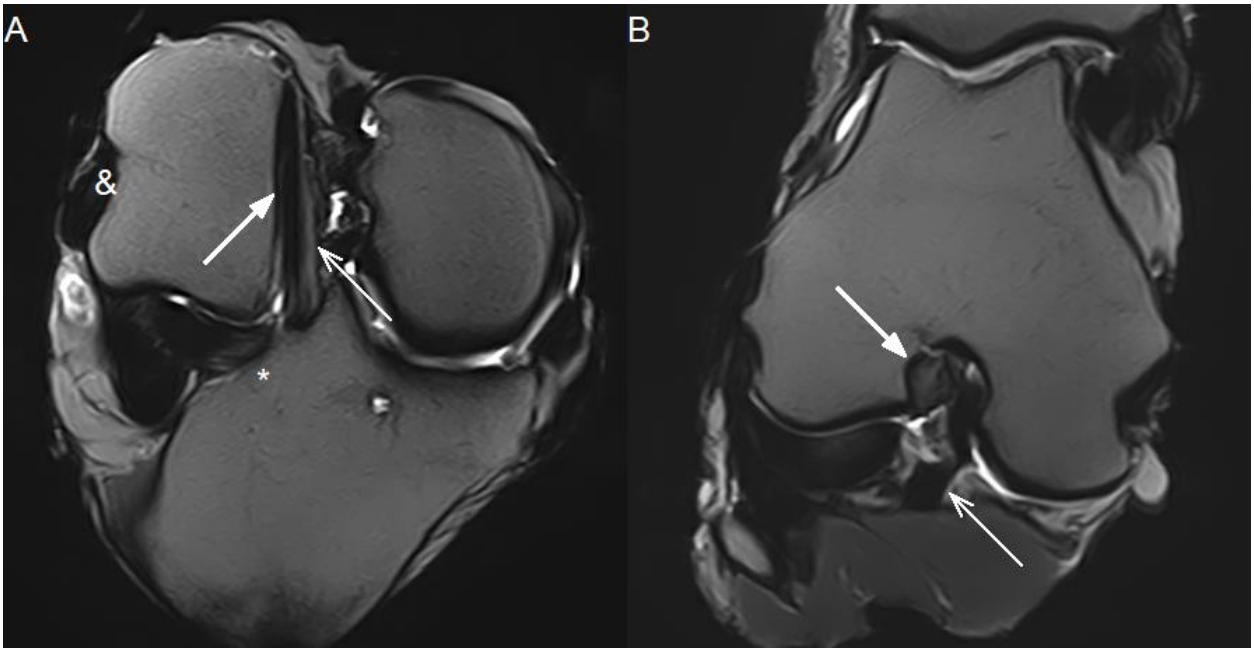

Figure 2: T2 weighted FSE MRI images of the cranial cruciate ligament. Medial is to the right of both images. A, Dorsal oblique plane image of horse 5 in the extended unloaded condition demonstrating the presence of a medial (open arrow) and lateral (closed arrow) bundle. The tibial insertion of the cranial ligament of the lateral meniscus is marked * and the femoral insertion of the popliteus tendon is marked &. B, Transverse oblique plane image of horse 6 in the extended unloaded condition showing the origin of the cranial cruciate ligament on the caudal axial aspect of the lateral femoral condyle with surrounding thin rim of low signal intensity (arrow). The tibial insertion of the caudal cruciate (open arrow) is obscured by the popliteus muscle.

In EXTLoad the two ligament regions were more clearly defined and distinct, although there was some variation in the degree of distinction between stifles. In EXTLoad, the lateral region was larger than the medial. The lateral region was homogenously hypointense and approximately the same width as the medial bundle for the proximal 75% and smaller for the distal 25%. There was minor individual variation in the width of the bundles within the ligament. The two regions appeared to be of approximately equal length in this condition. The remainder of the findings were unchanged from the extended unloaded condition.

In the FLEX condition the two regions could still be visualized, however the boundaries were less distinct and appeared more heterogenous than in the extended conditions. Both regions

had an undulant contour. The medial region appeared to make up a larger proportion of the ligament than in the extended conditions. The remainder of the findings were the same as the extended conditions.

The caudal cruciate ligament was best visualized on the T2 weighted FSE dorsal oblique and sagittal oblique sequences. In the EXT condition the ligament had a homogenously hypointense appearance with increased T2 signal intensity at the attachment on the femur (closed arrow, Figure 3A). The ligament origin was broad and fan-like. The cross-sectional shape became triangular then ovoid mid-body and then flattened into a broad flat oval at the insertion on the tibia. On the PD FSE sagittal sequence there was a linear hyperintensity within the distal third of the ligament at the level of the medial meniscus. On the cranial aspect of the caudal cruciate ligament at the level of the insertion there was a focal area of increased hyperintensity with a less compact fiber pattern. In EXTLoad the appearance of the ligament was the same as in EXT. In the FLEX condition the ligament continued to have a homogenously hypointense appearance, however the area of increased T2 signal intensity at the attachment on the femur extended further distally, continuing through the proximal third of the ligament in most stifles but occasionally extending further distally (Figure 3B). The remainder of the findings were unchanged from the extended conditions.

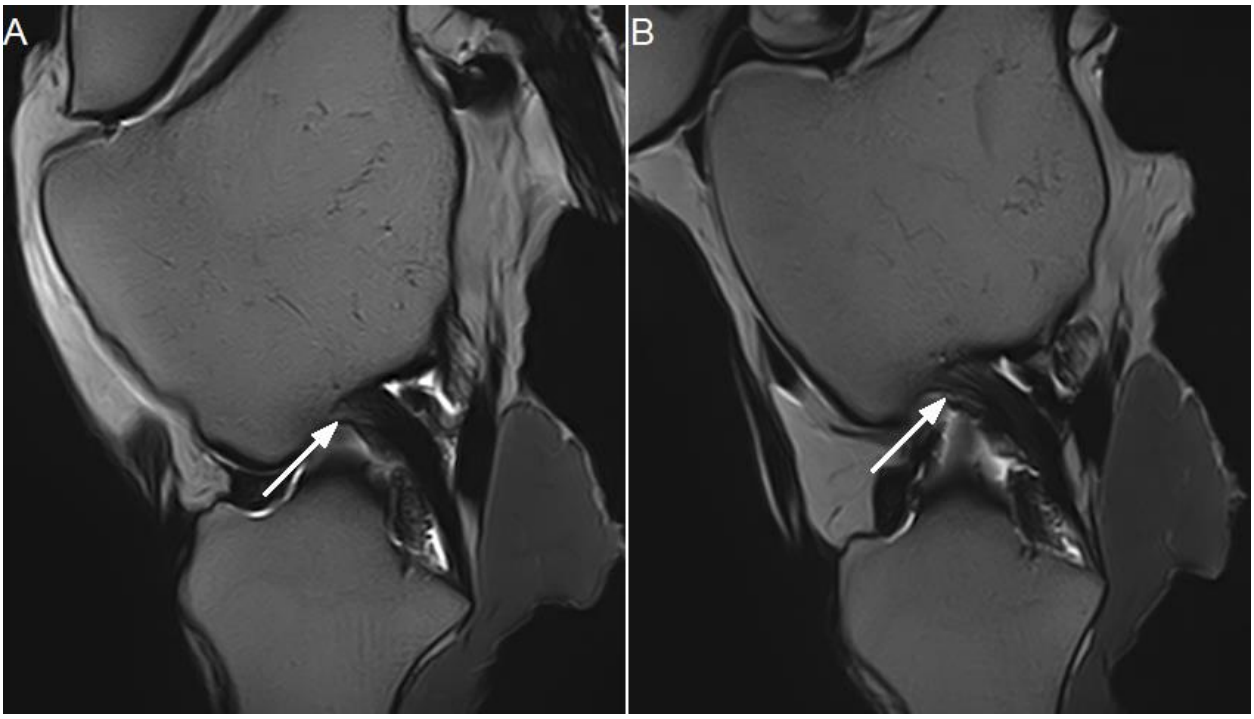

Figure 3: T2 weighted FSE MRI images of the caudal cruciate ligament. Cranial is to the left in both images. A, Sagittal oblique plane image of horse 6 in the extended unloaded condition showing the hypointense appearance of the caudal cruciate ligament (arrow) with an increased signal intensity at the femoral attachment. B, Sagittal oblique plane image of horse 6 in the flexed condition demonstrating the more distal extension of the increased signal intensity at the femoral attachment of the caudal cruciate ligament (arrow) in this condition.

Collateral ligaments

The collateral ligaments were best visualized on the transverse and dorsal PD weighted FSE sequences (Figure 9, Appendix A). In the EXT condition, the medial collateral ligament had a low overall signal intensity. On both the PD and T2 FSE images there was an increase in signal intensity at the origin on the medial femoral condyle. The medial collateral ligament was ovoid at its origin, becoming elongated as it crossed over the medial meniscus. A superficial and a deeper layer were apparent in the ligament distal to the level of the medial meniscus. The lateral collateral ligament was larger in cross section than the medial. It was triangular at the level of the meniscus and ovoid at the origin and insertion on the tibia and fibula. It had a low overall signal

intensity with an increased signal intensity at the origin on PD and T2 FSE images. Neither loading the stifle in extension nor flexing the stifle resulted in a change in the shape or signal intensity when compared to the EXT condition.

Menisci and associated ligaments

The menisci were best visualized on the dorsal and sagittal PD weighted FSE sequences. In the EXT condition, the medial meniscus had an overall low signal intensity with hyperintense curving striations at the medial, cranial, and caudal aspects that persisted on T2 FSE sequences and therefore were unlikely to be due to magic angle artifact (Figure 4 A-C). One horse had abnormalities consistent with a meniscal lesion and therefore could not be used for comparison. Description of these abnormalities was beyond the scope of this study. The lateral meniscus had an overall similar appearance to the medial meniscus with a generally low signal intensity. There were hyperintense horizontal curving striations at the lateral, cranial and caudal aspects of the meniscus (Figure 4 A-C). In the caudal aspect the hyperintensity resolved on T2 FSE sequences making this likely to be due to magic angle artifact, however the hyperintensity at the lateral and cranial aspects persisted on T2 FSE sequences. The close apposition of the lateral collateral ligament and popliteus tendon to the lateral meniscus caused the caudal and lateral margins of the lateral meniscus to be less clearly defined than the caudal and medial margins of the medial meniscus in all conditions. Loading the joint in extension did not result in changes to either meniscus.

Figure 4: PD weighted FSE dorsal plane MRI images of the medial (open arrow) and lateral (closed arrow) menisci in the extended unloaded condition from horse 6 demonstrating the hyperintense curving striations (collagen tie-fibers) at the abaxial, cranial and caudal aspects. Medial is to the right in all images. A, Cranial horns of the menisci. B, Midbodies of the menisci. C, Caudal horns of the menisci, * indicates the origin of the cranial cruciate ligament, the arrowhead the caudal cruciate ligament, and & indicates the meniscofemoral ligament.

The medial meniscus had a similar signal intensity in the FLEX and EXT conditions. In the FLEX condition on the PD FSE sagittal sequence, the cranial horn of the meniscus appeared subjectively slightly larger than in the extended conditions and was more triangular in appearance with less rounding of the cranial margin (Figure 5A-B). In the FLEX condition, the overall signal intensity and striations of the lateral meniscus were like in the EXT and EXTLoad conditions. In the FLEX condition the hyperintense curving striations at the caudal aspect did not resolve on T2 FSE sequences making it unlikely to be due to magic angle artifact. In the FLEX condition on the PD FSE sagittal sequence, the caudal horn of the lateral meniscus appeared subjectively slightly smaller than in the extended conditions while the cranial horn appeared more elongated and less round (Figure 5C-D).

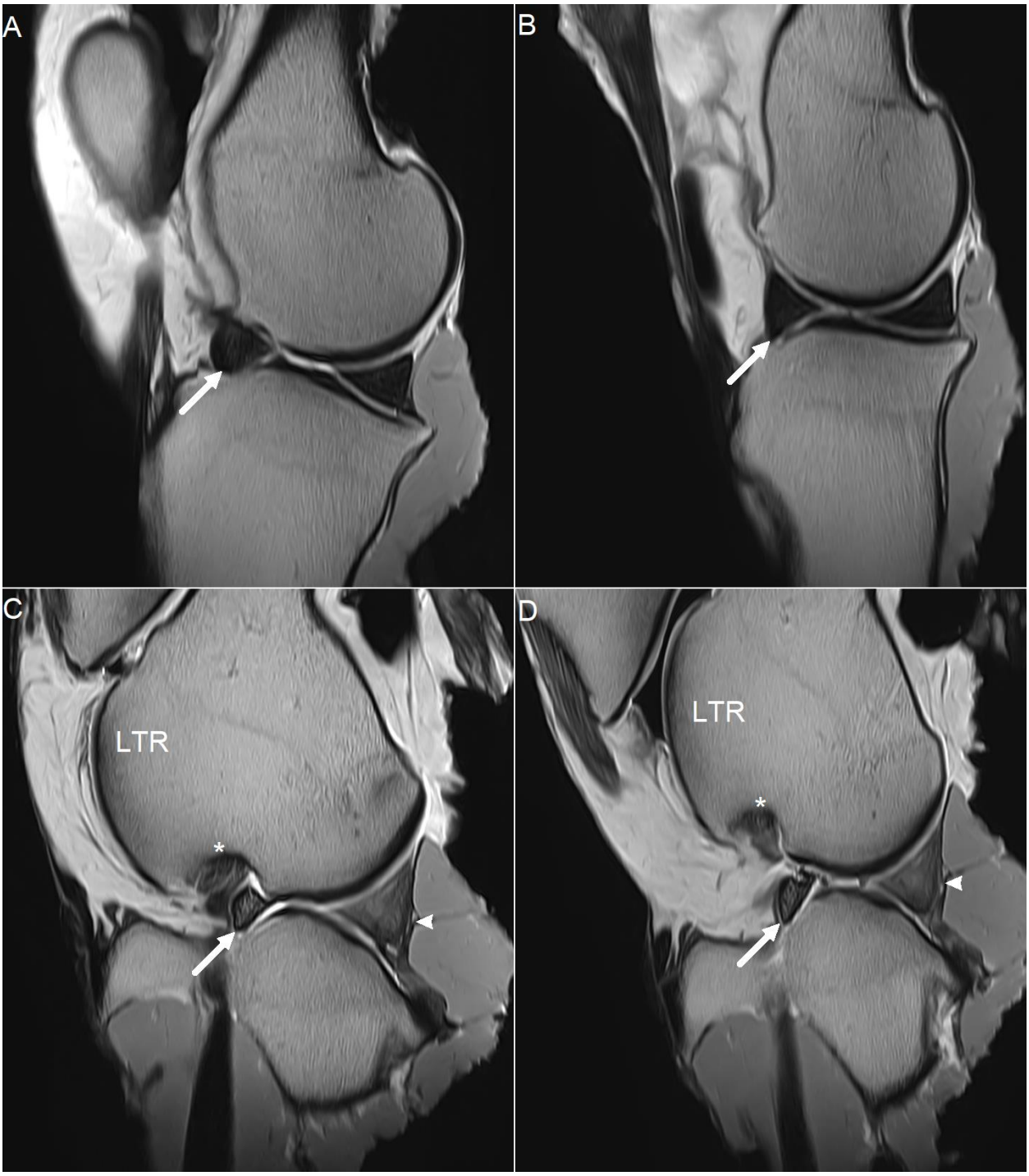

Figure 5: PD weighted FSE sagittal MRI images from horse 6. Cranial is to the left in all images. A, The medial meniscus (arrow) in the extended unloaded condition is more rounded at the cranial horn as compared to B, in the flexed condition. C, The cranial horn of the lateral meniscus (arrow) in the extended unloaded condition showing larger size and more rounding compared to D in the flexed condition. The caudal horn (arrowhead) is smaller and more hypointense in the flexed condition. *= origin of the peroneus tertius. LTR = lateral trochlear ridge.

The meniscotibial ligaments were best visualized on the transverse, dorsal and sagittal PD weighted FSE sequences. The caudal medial meniscotibial ligament was hypointense with prominent horizontal hyperintense striations best observed on dorsal and transverse planes. These striations gave the ligament a stippled appearance on sagittal plane images. The cranial medial meniscotibial ligament was similar in appearance to the caudal but was wider and shorter. Loading the joint had no effect on the appearance of either of the medial meniscotibial ligaments. In extension the cranial medial ligament was more flattened with a proximal concavity secondary to compression from the medial femoral condyle in comparison to the flexed condition. Flexion had no other effects on either medial meniscotibial ligament.

The cranial lateral meniscotibial ligament had a similar intensity and striations to the cranial medial ligament and an increased number of hyperintense striations resulting in a more intermediate signal intensity. The lateral ligament attached on the tibia at a slightly more caudal location than the medial. The caudal lateral meniscotibial ligament was similar in appearance to the medial but was narrower and less distinct with less distinct striations. The caudal lateral ligament attached more caudally on the tibia than did the medial. Loading the joint had no effect on the appearance of either of the lateral meniscotibial ligaments. Flexion caused the striations of the cranial ligament to become slightly less hyperintense and distinct but had no effect on the caudal ligament.

The meniscofemoral ligament was best visualized on the transverse, dorsal and sagittal PD weighted FSE sequences. In the EXT condition, the ligament was hypointense with numerous, hyperintense curving, linear striations best visualized on the dorsal plane images. On transverse plane images the striations gave the ligament a stippled appearance. The junction between the ligament and the lateral meniscus was distinct. Loading the joint did not change the

meniscofemoral ligament. Flexion of the stifle caused the striations to appear more linear and organized.

Distal patellar ligaments

The distal patellar ligaments were best visualized on the transverse, dorsal and sagittal PD weighted FSE sequences. The lateral patellar ligament had a uniformly low signal intensity throughout its length with multiple hyperintense clefts extending into the caudoaxial aspect of the ligament within its distal third, best appreciated in the transverse plane. The ligament was broad and flat throughout its length although it became somewhat more rounded in the distal third. EXTload did not change the appearance of the ligament. Flexing the stifle caused the hyperintense clefts in the distal ligament to become thinner and more tapered. The ligament overall developed a mildly undulant contour, most pronounced distally.

In the EXT condition the middle distal patellar ligament had a low overall signal intensity with hyperintense longitudinal striations present throughout the length of the ligament. The ligament had a flattened ovoid shape throughout its length, particularly where it contacted the medial trochlear ridge where the striations also became less prominent, except within the distal aspect of the ligament where it became rounded before inserting on the proximal tibia. The ligament was surrounded by the infrapatellar fat pad except where the caudal aspect was in contact with the medial trochlear ridge. The EXTLoad condition did not change the appearance of the middle patellar ligament. Flexion of the joint resulted in the striations becoming less well defined, particularly in the distal half of the ligament. Flexion also resulted in loss of contact with the medial trochlear ridge such that the ligament was surrounded by the infrapatellar fat pad throughout its length due to the more cranial and distal position of the patella during flexion.

The medial patellar ligament in EXT was uniformly hypointense except in the distal aspect where there were multiple hyperintense clefts extending into the caudoaxial aspect of the ligament prior to its insertion on the tibia. While wide at its origin on the patellar fibrocartilage, the ligament rapidly narrowed and became ovoid throughout the remainder of its length. Loading the stifle did not result in any changes to the medial patellar ligament. Flexion of the joint resulted in the ligament moving to a more cranial position within the stifle but no other changes.

Quantitative Ligament Evaluation

The results of the linear mixed models are presented in Table 6, Appendix A. The results of the pairwise comparisons between treatments for measurements which had significant treatment effects are presented in Table 7, Appendix A.

Cruciate ligament measurements

The three conditions (EXT, EXTLoad, and FLEX) did not affect the length or CSA of the cruciate ligaments (Table 2). The tibial angle of insertion of the cruciate ligaments was not different for either extended condition, however when flexed, the tibial angle of insertion for the cranial cruciate ligament was significantly smaller ($P<0.01$) and for the caudal cruciate ligament was significantly larger ($P<0.01$).

Table 2: Mean ± standard deviation values for the length, mid-ligament cross-sectional area, and tibial angle of insertion for the cranial and caudal cruciate ligaments. CSA=cross-sectional area.

	Cranial Cruciate Ligament			Caudal Cruciate Ligament		
	Length (mm)	CSA (mm^2)	Tibial Angle (degrees)	Length (mm)	CSA (mm^2)	Tibial Angle (degrees)
Extended	55.01 ± 4.0	102.36 ± 27.6	73.72 ± 6.6[a]	56.53 ± 5.5	63.60 ± 9.7	30.452 ± 6.8[c]
Extended-Loaded	54.54 ± 4.5	104.64 ± 39.6	75.47 ± 7.3[a]	56.40 ± 2.8	67.60 ± 9.1	31.77 ± 5.0[c]
Flexed	55.57 ± 5.3	112.22 ± 30.3	56.01 ± 8.2[b]	56.88 ± 3.9	58.94 ± 7.3	41.76 ± 3.1[d]

Different lettered superscripts indicate significant differences between conditions ($P<0.05$)

Collateral ligament measurements

The three conditions did not affect the CSA of the medial collateral ligament (Table 3). The medial collateral ligament was significantly longer in the FLEX condition when compared to the EXTLoad condition ($P=0.035$), but the length was not different between the other conditions. For the lateral collateral ligament there was no difference in length between the three conditions however, the CSA of the lateral collateral ligament in the flexed condition was greater than in the EXT or EXTload conditions ($P<0.05$).

Table 3: Mean ± standard deviation values for the length and mid-ligament cross-sectional area for the medial and lateral collateral ligaments. CSA=cross-sectional area.

	Medial Collateral		Lateral Collateral	
	Length (mm)	CSA (mm^2)	Length (mm)	CSA (mm^2)
Extended	$73.59 \pm 8.1^{a,b}$	38.77 ± 9.2	81.62 ± 8.3	70.24 ± 13.6^{c}
Extended-Loaded	72.09 ± 10.0^{a}	36.32 ± 15.6	79.53 ± 7.5	68.38 ± 9.9^{c}
Flexed	77.68 ± 6.8^{b}	36.10 ± 11.0	79.45 ± 5.8	79.34 ± 12.3^{d}

Different letter superscripts indicate significant differences between conditions ($P<0.05$)

Meniscal cross-sectional area

Condition affected some CSA measurements of the medial meniscus (Table 4). The CSA of the cranial horn in the FLEX condition was greater than EXT ($P=0.03$). The CSA of EXTLoad was not different from either EXT or FLEX conditions. At midbody, the CSA in the FLEX condition was greater ($P<0.03$) than EXT or EXTLoad which were the same. The caudal horn CSA was smaller in FLEX than EXTLoad ($P<0.01$) but not EXT. There was no difference in caudal horn CSA between EXT and EXTLoad. Condition affected some CSA location measurements of the lateral meniscus (Table 4); however, the CSA of the cranial horn was not affected. The CSA of the midbody and the caudal horn was smaller in FLEX than in EXT and EXTLoad conditions ($P<0.03$) which were the same.

Table 4: Mean ± standard deviation values for the cross-sectional area (mm^2) of the medial and lateral menisci at the level of the cranial and caudal horns as well as the mid-body.

	Medial Meniscus			Lateral Meniscus		
	Cranial Horn	Midbody	Caudal Horn	Cranial Horn	Midbody	Caudal Horn
Extended	270.10 ± 51.6[a]	109.92 ± 17.3[c]	377.53 ± 22.8[e,f]	336.46 ± 71.3	134.92 ± 16.9[g]	520.47 ± 49.2[i]
Extended-Loaded	281.53 ± 71.0[a,b]	100.59 ± 10.3[c]	386.91 ± 24.8[e]	294.84 ± 61.2	140.21 ± 15.6[g]	527.61 ± 87.3[i]
Flexed	316.24 ± 50.2[b]	153.38 ± 50.0[d]	357.87 ± 34.9[f]	341.75 ± 21.9	128.29 ± 12.4[h]	411.38 ± 81.7[j]

Different letter superscripts indicate significant differences between conditions ($P<0.05$)

Histologic analysis

The collected samples were suitable for histological analysis and no histologic abnormalities were identified. Both the medial and lateral collateral ligaments were uniform in appearance with a consistent linear collagen fiber pattern. Two distinct collagen fiber patterns, organized in discrete directions, were visible and most evident on the sagittal sections of both the cranial and caudal cruciate ligaments (Figure 6, Figure 7). In both ligaments, the lateral bundle had a more distinctly longitudinal fiber pattern with a dense array of collagen fibers. The medial bundle had fibers oriented obliquely to the longitudinal axis of ligament and these fibers were much less densely arranged. The medial and lateral bundles of collagen fibers were interspersed with connective tissue containing abundant cells. Ligamentocytes were also visible on the surface of the fibers.

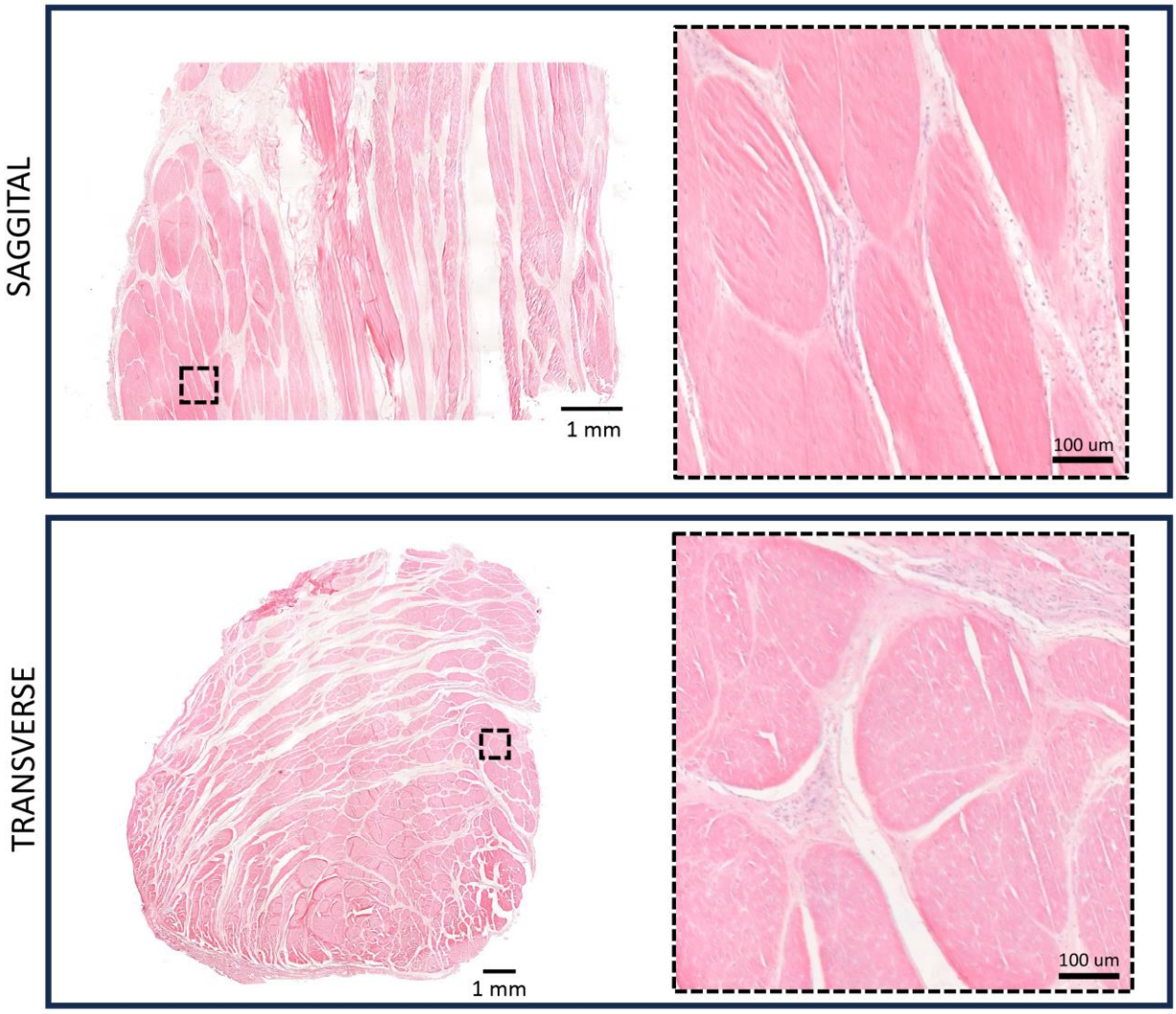

Figure 6: Sagittal and transverse sections of a normal cranial cruciate ligament stained with hematoxylin and eosin. Magnified focal areas (broken black square) in right panel, demonstrate the collagen fiber organization. Sagittal section: The lefthand image illustrates two collagen organization patterns with distinct alignments composing the medial and lateral bundles, with surrounding connective tissue. The magnified focal area (broken black square) in the right panel demonstrates the collagen fiber organization in the medial bundle. Additionally, the extensive cellularity (blue stained nuclei) of the connective tissue is also visible. Transverse section: Variations in the structural organization of the collagen are also evident but are not as clearly defined as in the sagittal section.

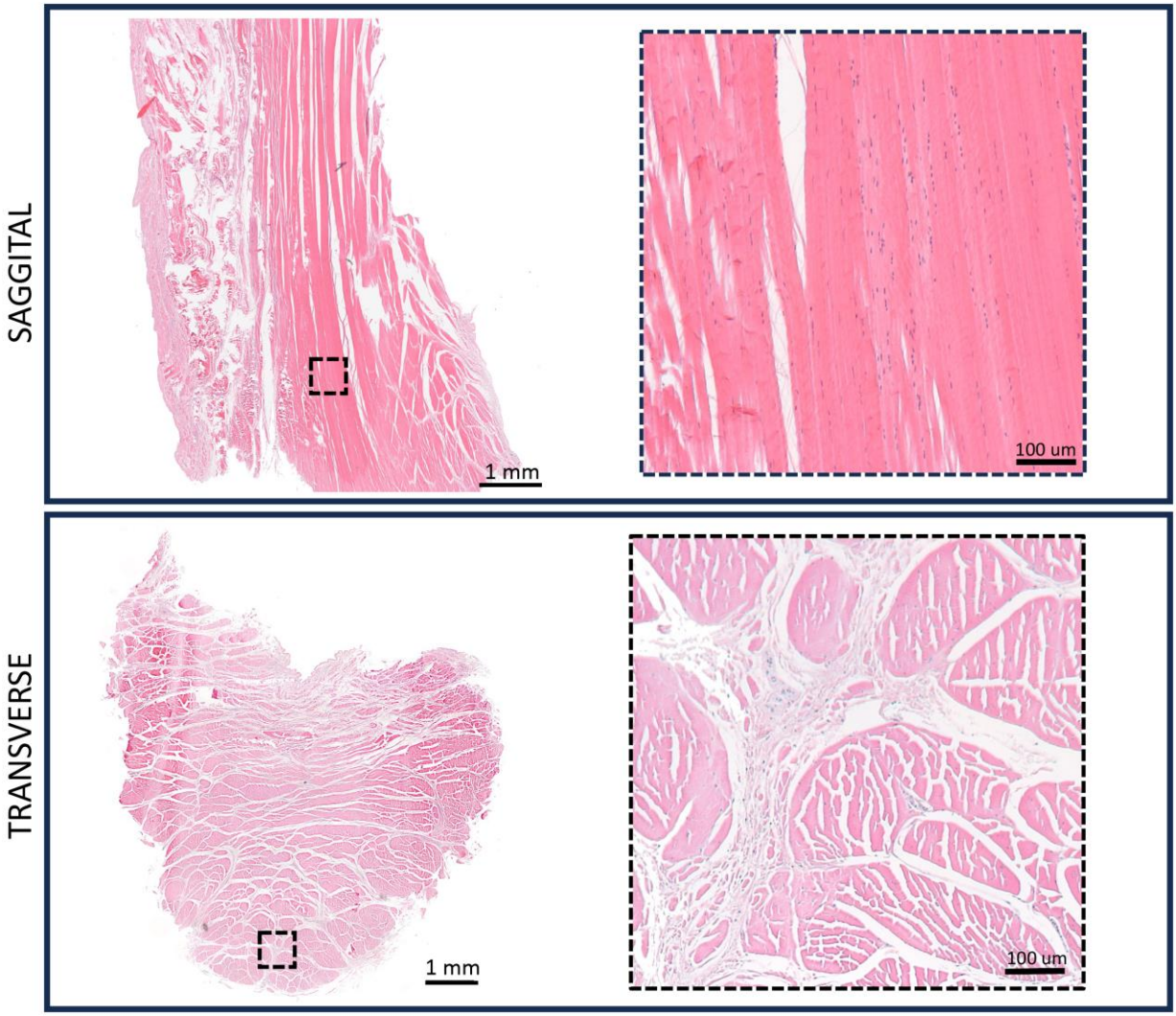

Figure 7: Sagittal and transverse sections of a normal caudal cruciate ligament stained with hematoxylin and eosin. Magnified focal areas (broken black square) in right panel, demonstrate the collagen fiber organization. Sagittal section: The lefthand image illustrates the two distinct collagen organization patterns of the medial and lateral bundles with surrounding connective tissue. Artefactual separation of the fibers is evident in the left part of the image. The magnified focal area (broken black square) in the right panel demonstrates the longitudinal collagen fiber organization in the lateral bundle. Ligamentocytes are visible within the ligament tissue. Transverse section: Variations in the structural organization of the collagen are also evident in this section but are not as clearly defined as in the sagittal section.

Chapter 4 - Discussion

The equine stifle is a highly complex and dynamic joint, and soft tissue injuries occur during specific joint conditions (22). The contribution of soft tissue injuries to stifle-associated lameness in the horse results in a need to understand the MRI anatomy of the equine stifle and its relation to injury and performance (3). Imaging the stifle in different conditions has the potential to improve our understanding of the biomechanics of stifle injuries. The results presented here describe the soft tissues of the stifle under simulated loading conditions with the joint in flexion and extension. This model only captures limited positions and small loads but does offer a snapshot of the joint in motion and has the potential to be a fuller representation of the joint in vivo. The application of more advanced techniques, such as dynamic MRI as used in the imaging of human joints including the knee, could allow for a more comprehensive evaluation of the stifle throughout its range of motion, should this technology become feasible in veterinary medicine (20, 21, 23). To the authors' knowledge, this is the first published report to incorporate these features into magnetic resonance imaging of the equine stifle. Furthermore, it is the first to describe the presence of two distinct regions of intensity and collagen fiber patterns, consistent with the bundles described in human knees, in the cruciate ligaments (18, 19).

The only cruciate ligament metric affected by stifle flexion was the tibial angle of insertion, which decreased for the cranial and increased for the caudal cruciate ligament. These changes are intuitive given the origin and insertion of the cruciate ligaments and how these relationships change during flexion and extension. It is interesting that none of the other measured parameters changed with flexion given that it has been reported in the human literature that the distances between the points of origin and insertion of the cranial and caudal cruciate ligaments change with flexion and extension (17). However, the equine femur and tibia are

connected much closer than in the human knee as evidenced by a reduced ability to visualize equine stifle structures during ultrasound and arthroscopy (4, 6, 11). It is likely that the equine cruciate ligaments are less elastic resulting in reduced ligament lengthening.

The most noteworthy finding when evaluating the cruciate ligaments was the identification of two distinct regions of intensity in the ligament, consistent with the presence of distinct bundles. This has been established in human medicine (18, 19) but has not yet been described in the equine stifle literature. The most recent descriptive study on MRI of the equine stifle did not provide sufficient image detail to evaluate cruciate ligament fiber composition and alignment (15). This is a novel finding that has the potential to alter how we think about the cruciate ligaments of the stifle and how they should be evaluated by MRI and managed in cases of injury.

The MRI appearance of these bundles in the cranial cruciate ligament in the present study correlated well with the description of the human cranial/anterior cruciate ligament. In both species the medial bundle maintains a more cranial/anterior position and tibial insertion compared to the lateral bundle (18). The MRI presence of two distinct bundles in the cranial cruciate ligament was further reinforced by the histology of the ligament which clearly showed two distinct bundles with differing collagen fiber patterns. This suggests that the bundles seen on MRI were not artifactual and do reflect structural differences in fiber orientation and density within the ligament.

In humans, passive flexion and extension of the knee has different effects on the tensioning of the two bundles of the cranial cruciate ligament resulting in differing functions. Extension of the knee results in tightening of the posterolateral bundle and moderate laxity of the anteromedial bundle, while flexion has the opposite effect (18, 24). In the current study, flexion

of the stifle resulted in minor, subjective changes in the appearance of the two bundles. Some of these changes may be due to slight differences in the angle of the MRI slices during flexion as compared to extension, but the undulant contour of the bundles suggests increased laxity in the flexed condition. Furthermore, the proportionally increased cross-sectional area of the medial bundle relative to the lateral could indicate that the medial bundle is more lax in flexion, contrary to what has been described in the human knee. Since the cross-sectional area of each bundle was not measured in this study it is not possible to say if these subjective differences were statistically significant, but this suggests a potential area of future research. The presence of two bundles as well as the possibility that they serve distinct functions could also have implications for the prognosis of horses with cranial cruciate injuries depending on the bundle affected. These bundles may also play a role in the pathogenesis of cranial cruciate ligament injuries in the horse as well as the location of tears within this ligament.

In contrast to the cranial cruciate ligament, the caudal cruciate ligament did not show evidence of distinct bundles on MRI (Figure 8). In all conditions the ligament appeared as a homogenously T2 hypointense structure, which contrasts with the caudal/posterior cruciate ligament of the human knee which consists of anterolateral and posteromedial bundles with distinct mechanical properties (19). Contrary to the MRI findings, histology of the caudal cruciate ligament did demonstrate two bundles. The most likely explanations for the contradictory findings between histology and MRI may be due to partial volume averaging secondary to the 2 mm slice thickness obscuring the distinction between the bundles, and/or the obliquity of the MRI slices relative to the bundles preventing distinguishing between them. However, it is not possible to rule out error in interpretation of the histologic findings. In some specimens, when the stifle was subjected to flexion, the region of increased T2 signal intensity

seen at the attachment on the femur extended distally through the ligament, almost to its tibial insertion, and it is possible that this hyperintensity could represent a second bundle in the ligament that was only visible in some stifles.

Figure 8: PD weighted transverse plane MRI image immediately distal to the femoral epicondylar fossa. Medial is to the left. The closed arrow indicates the cranial cruciate ligament with its two bundles. The bracket indicates the broad femoral origin of the caudal cruciate ligament, the * indicates the medial collateral ligament and the arrowhead indicates the lateral collateral ligament.

The collateral ligaments were uniform in structure and appearance on histology and MRI, and were made up of a single bundle, consistent with previous descriptions (3). This differs from the collateral ligaments in humans where the medial collateral has deep and superficial portions and both the lateral collateral and superficial component of the medial collateral are sometimes further subdivided into anterior, middle, and posterior bundles (25). These bundles have been shown in humans to have distinct functional roles (25). In flexion, the lengthening of the medial collateral ligament and the increase in area of the lateral in this study also suggests differing actions. It is possible that the equine collateral ligaments have similarly functionally distinct components but that they are not structurally distinguishable, however this would require further exploration.

Both the medial and lateral menisci showed striations on MRI that were consistent with the appearance of normal meniscal collagen tie-fibers as have been previously demonstrated (26-28). These striations can make it difficult to identify horizontal tears of the outer border of the meniscus on MRI as the two can appear similar (29). The medial and lateral menisci also showed the most changes in the measured parameters. For both menisci, the cross-sectional area of the caudal horn decreased during joint flexion. This agrees with a previous study that evaluated equine meniscal function that showed stifle flexion results in a caudal shift in contact pressure on the medial tibial condyle, likely compressing the caudal horn (30).

The cross-sectional area of the cranial horn of the medial meniscus increased in the FLEX condition. The cranial horn of the medial meniscus is the least mobile of the four meniscal horns (22). It is possible that this decreased capacity for translocation results in less compressive force on the cranial horn during flexion as the pressure on the medial tibial condyle shifts caudally, resulting in an increase in cross-sectional area (30). The cranial horn of the lateral

meniscus in contrast has substantial caudal translocation during stifle flexion and therefore may experience a smaller decrease in compressive force with flexion, resulting in minimal change in cross-sectional area (22). In this study the cranial horn of the medial meniscus showed the greatest decrease in cross-sectional area during extension. Medial meniscal injuries are also the most diagnosed meniscal injury in the horse, making up 60-83% of meniscal injuries (31-34). A proposed mechanism of meniscal injuries in horses is compression of the cranial horn between the femur and the tibia during extension (22), which could account for the decrease in cross-sectional area in this study.

The CSA of the midbody of the menisci in FLEX condition decreased for the lateral meniscus and increased for the medial meniscus as compared to both extended conditions. This suggests that the menisci of the equine stifle function independently and are biomechanically distinct. While multiple studies have demonstrated that the majority of arthroscopically diagnosed equine meniscal injuries occur in the cranial horn of the medial meniscus, there are no comparative studies between menisci regarding outcomes nor have any studies specifically described the most common location of lateral meniscal tears (31-34). This is further complicated by the limited ability to evaluate the lateral meniscus in the horse both arthroscopically and ultrasonographically (4). It is unclear if the decrease in cross-sectional area at the midbody and caudal horn of the lateral meniscus during flexion increases the risk of injury to these regions.

Changing the load on the stifle in extension had no effect on any measured parameters, suggesting either there was insufficient load applied across the stifle or that loading the stifle does not affect the position or geometry of the femorotibial ligaments. The peak ground reaction force on the hindlimb of an average light breed horse at the walk has been calculated at 1800 N

(30). The force of 138 N applied across the stifle was as much as was possible without using ferromagnetic materials. Given that this force is an order of magnitude smaller than the physiologic load across the stifle joint at the walk, it is most likely that this force was insufficient to generate measurable changes in the structures evaluated. Future studies could identify a way to apply greater force across the stifle joint without ferrous components allowing MRI to be performed to evaluate the soft tissues of the joint.

Other limitations of this study include the use of cadaveric, refrigerated stifles which limits the ability to generalize the current findings to in vivo scenarios. Additionally, removing the periarticular soft tissues could change how the tissues of the stifle respond to load and flexion. These limitations were mitigated as much as possible by ensuring that the popliteus tendon, collateral ligaments, distal patellar ligaments, and joint capsule were left intact and by simulating the effect of the quadriceps muscle on the patella with the proximal cable tie. Measurements were obtained at select sites and do not fully describe the changes that occur during flexion and loading of the equine stifle. Taking measurements at more sites could potentially reveal further changes in the femorotibial ligaments, and increasing the sample size would also increase our ability to identify differences in the measurements of these ligaments.

In conclusion, 3 T MRI of the equine stifle enables detailed evaluation of the cruciate ligaments of the equine stifle, revealing the presence of two distinct bundles making up the cranial cruciate ligament. This finding was confirmed on histologic evaluation. Histologically, the caudal cruciate ligament also had two bundles, but these could not be identified on MRI. Stifle flexion altered the tibial angles of attachment for the cruciate ligaments, increased the length of the medial collateral ligament and the cross-sectional area of the lateral, and altered the cross-sectional area of all measured aspects of the menisci excepting the cranial horn of the

lateral meniscus. These changes demonstrate the dynamic nature and complexity of the equine stifle soft tissue components and could suggest the etiopathogeneses of injury. Future studies are needed to correlate these findings with clinical stifle injuries.

References

1. Singer ER, Barnes J, Saxby F, Murray JK. Injuries in the event horse: Training versus competition. *The Veterinary Journal* 2008; 175: 76-81.

2. Dyson SJ. Lameness associated with the stifle and pelvic regions. In: Proceedings, 48th Annual Meeting of American Association of Equine Practice 2002; 387-411.

3. Fowlie JG, Richardson DW, Ortved KF. Chapter 101 - Stifle. In: Equine Surgery (Fifth Edition). WB Saunders; 2019; 1747-1777.

4. Barrett MF, Frisbie DD, McIlwraith CW, Werpy NM. The arthroscopic and ultrasonographic boundaries of the equine femorotibial joints. *Equine Veterinary Journal* 2012; 44: 57-63.

5. Crijns CP, Gielen IMVL, Van Bree HJJ, Bergman EHJ. The use of CT and CT arthrography in diagnosing equine stifle injury in a Rheinlander gelding. *Equine Veterinary Journal* 2010; 42(4): 367-371.

6. Maulet BEB, Mayhew IG, Jones E, Booth TM. Radiographic anatomy of the soft tissue attachments of the equine stifle. *Equine Veterinary Journal* 2005; 37(6): 530-535.

7. Nelson BB, Kawcak CE, Goodrich LR, Werpy NM, Valdes-Martinez A, McIlwraith CW. Comparison between computed tomographic arthrography, radiography, ultrasonography, and arthroscopy for the diagnosis of femorotibial joint disease in western performance horses. *Vet Radiol Ultrasound* 2016; 57(4): 387-402.

8. Dik KJ. Ultrasonography of the equine stifle. *Equine Veterinary Education* 1995; 7: 154-160.

9. Trencart P, Alexander K, De Lasalle J, Laverty, S. Radiographic evaluation of the width of the femorotibial joint space in horses. *American Journal of Veterinary Research* 2016; 77(2): 127-136.

10. De Lasalle J, Alexander K, Olive J, Laverty S. Comparisons among radiography, ultrasonography and computed tomography for ex vivo characterization of stifle osteoarthritis in the horse. *Vet Radiol Ultrasound* 2016: 57(5): 489-501.

11. Adrian AM, Barrett MF, Werpy NM, Kawcak CE, Chapman PL, Goodrich LR. A comparison of arthroscopy to ultrasonography for identification of pathology of the equine stifle. *Equine Veterinary Journal* 2017; 49: 314-321.

12. Nagy A, Dyson S. Magnetic resonance imaging and histological findings in the proximal aspect of the suspensory ligament of forelimbs in nonlame horses. *Equine Veterinary Journal* 2012; 44: 43-50.

13. Nacey NC, Geeslin MG, Miller GW, Pierce JL. Magnetic resonance imaging of the knee: An overview and update of conventional and state of the art imaging. *J Magn Reason Imaging* 2017; 45: 1257-1275.

14. Judy CE. Magnetic resonance imaging of the equine stifle in a clinical setting. *Proc ACVS* 2007; 36: 163-166.

15. Daglish J, Frisbie DD, Selberg KT, Barrett MF. High field magnetic resonance imaging is comparable with gross anatomy for description of the normal appearance of soft tissues in the equine stifle. *Veterinary Radiology & Ultrasound* 2018; 59: 721-736.

16. Abmann AD, Ohlerth S, Sanchez-Andrade JS, Torgerson PR, Bischofberger AS. Ex vivo comparison of 3 Tesla magnetic resonance imaging and multidetector computed tomography arthrography to identify artificial soft tissue lesions in equine stifles. *Veterinary Surgery* 2022; 51: 648-657.

17. Fuss FK. Anatomy of the cruciate ligaments and their function in extension and flexion of the knee joint, *Am J Anat* 1989; 184: 165-176.

18. Zantop T, Herbort M, Raschke MJ, Fu FH, Petersen W. The role of the anteromedial and posterolateral bundles of the anterior cruciate ligament in anterior tibial translation and internal rotation. *The American Journal of Sports Medicine* 2007; 35(2): 223-227.

19. Race A, Amis AA. The mechanical properties of the two bundles of the human posterior cruciate ligament. *Journal of Biomechanics* 1994; 27(1): 13-24.

20. Vedi V. Meniscal movement. *The Journal of Bone & Joint Surgery British Volume* 1999; 81-B(1): 37-41.

21. Westphal J, Schmitz A, Reeder SB, Thelen DG. Load-dependent variations in knee kinematics measured with dynamic MRI. *Journal of Biomechanics* 2013; 46(12): 2045-2052.

22. Fowlie JG, Arnoczky P, Stick JA, Pease AP. Meniscal translocation and deformation throughout the range of motion of the equine stifle joint: An *in vitro* cadaveric study. *Equine Veterinary Journal* 2011; 43(3): 259-264.

23. Garetier M, Borotikar B, Makki K, Brochard S, Rousseau R, Ben Salem D. Dynamic MRI for articulating joint evaluation on 1.5 T and 3.0 T scanners: setup, protocols, and real-time sequences. *Insights into Imaging* 2020; 11(1): 66.

24. Petersen W, Tillmann B. Anatomy and function of the anterior cruciate ligament. *Orthopade* 2002; 31: 710-718.

25. Park SE, DeFrate LE, Suggs JF, Gill TJ, Rubash HE, Li G. Erratum to “The change in length of the medial and lateral collateral ligaments during in vivo knee flexion”. *The Knee* 2006; 13(1): 77-82.

26. Dubuc J, Moser T, Laverty S. Comparative study of the ultrasonographic examination, magnetic resonance imaging, and histology of the equine meniscus – Preliminary findings. In: Scientific Presentation Abstracts: 2019 European College Veterinary Surgeons 28th Annual Scientific Meeting; July 2-4, 2019; Budapest, Hungary.

27. Andrews SH, Rattner JB, Abusara Z, Adesida A, Shrive NG, Ronsky JL. Tie-fibre structure and organization in the knee menisci. *Journal of Anatomy* 2014; 224(5): 531-537.

28. Pinsard M, Laverty W, Richard H, Dubuc J, Schanne-Klein M, Legare F. Maturation of the meniscal collagen structure revealed by polarization-resolved and directional second harmonic generation microscopy. *Scientific Reports* 2019; 9, 18448.

29. Tuckman GA, Miller WJ, Remo JW, Fritts HM, Rozansky MI. Radial tears of the menisci: MR findings. *American Journal of Roentgenology* 1994; 163(2): 395-400.

30. Fowlie J, Arnoczky S, Lavagnino M, Maerz T, Stick J. Resection of grade III cranial horn tears of the equine medial meniscus alter the contact forces on medial tibial condyle at full extension: An in-vitro cadaveric study. *Veterinary Surgery* 2011; 40(8): 909-1032.

31. Cohen JM, Richardson DW, McKnight AL, Ross MW, Boston RC. Long-term outcome in 44 horses with stifle lameness after arthroscopic exploration and debridement. *Veterinary Surgery* 2009; 38(4): 543-551.

32. Walmsley P, Phillips TJ, Townsend GG. Meniscal tears in horses: an evaluation of clinical signs and arthroscopic treatment of 80 cases. *Equine Veterinary Journal* 2003; 35(4): 402-406.

33. Davis JG, Garcia JM. Arthroscopic findings and long-term outcomes in 76 sporthorses with meniscal injuries (2008-2018). *Veterinary Surgery* 2022; 51: 409-417.

34. Dubuc J, Girard C, Richard H, De Lasalle J, Laverty S. Equine meniscal degeneration is associated with medial femorotibial osteoarthritis. *Equine Veterinary Journal* 2018; 50(1): 133-140.

Appendix A - Supplemental Tables and Figures

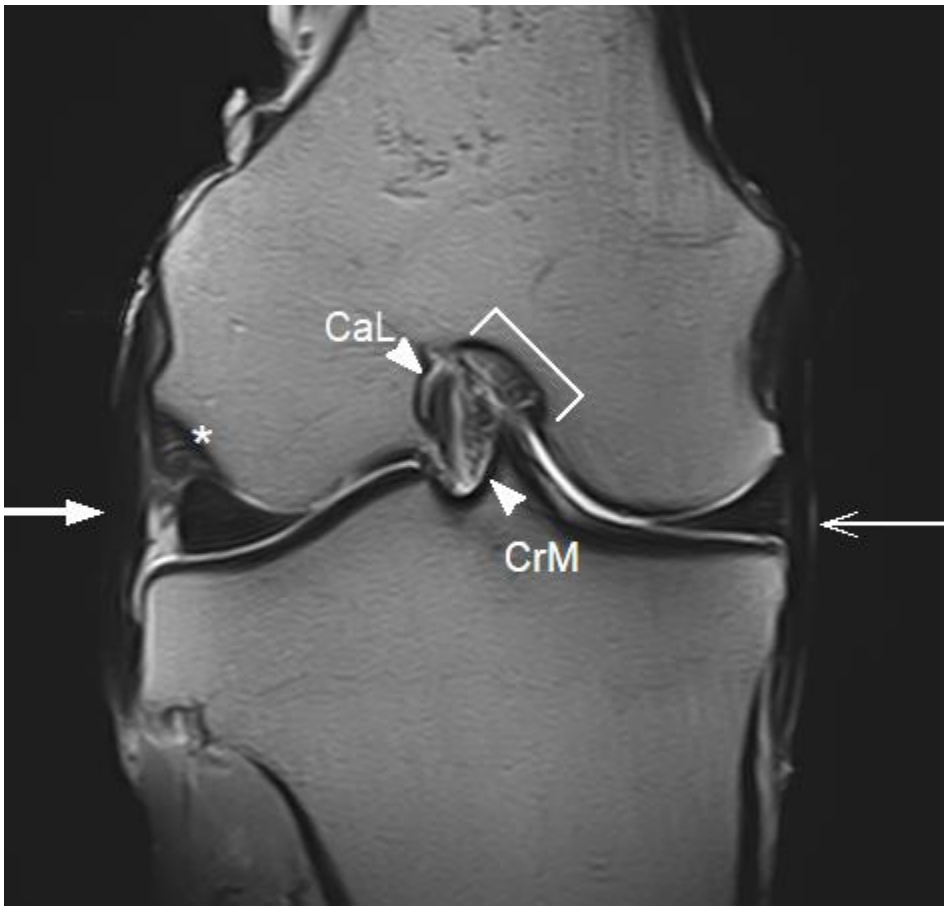

Figure 9: PD weighted FSE dorsal plane MRI image of the collateral ligaments in the extended unloaded condition from horse 6. Medial is to the right. Both the medial (open arrow) and lateral (closed arrow) collateral ligaments demonstrate a low overall signal intensity with increased signal intensity at the origins. The two bundles of the cranial cruciate ligament are apparent (arrowheads) as is the origin of the caudal cruciate ligament on the proximal intercondylar fossa (bracket). The attachment of the popliteus tendon is indicated by *. CaL = caudolateral, CrM = craniomedial.

Table 5: Mean measurements of ligament length (mm), tibial angle (degrees), and cross-sectional area (mm^2) for all horses under the three conditions (EXT, EXTLoad, and FLEX). Reported are the means of the three measured values for each structure. CSA=cross-sectional area.

		Cranial Cruciate Ligament			Caudal Cruciate Ligament			Medial Collateral Ligament		Lateral Collateral Ligament		Medial Meniscus			Lateral Meniscus		
Horse	Treatment	Length	Tibial angle	CSA	Length	Tibial angle	CSA	Length	CSA	Length	CSA	CSA: Cranial horn	CSA: Midbody	CSA: Caudal horn	CSA: Cranial horn	CSA: Midbody	CSA: Caudal horn
1	EXT	56.7	70.0	102.9	62.0	24.9	51.0	69.6	36.4	82.3	64.6	206.2	117.0	376.6	343.6	132.9	561.5
	EXTLoad	60.3	69.3	93.2	59.0	26.1	53.8	64.0	26.3	86.1	63.7	243.7	106.8	394.2	290.9	145.2	500.6
	FLEX	59.0	45.4	67.3	57.6	42.2	55.3	74.4	28.3	71.1	64.7	253.9	242.8	362.5	344.3	125.0	392.8
2	EXT	55.0	69.0	59.4	54.7	31.3	66.0	61.1	21.3	88.2	46.4	239.5	89.2	350.4	215.9	106.0	436.7
	EXTLoad	49.8	68.7	52.7	53.6	31.9	75.5	59.3	9.6	89.9	54.9	201.6	105.4	342.0	195.4	109.3	408.8
	FLEX	55.8	52.8	117.1	50.6	41.3	51.0	67.6	17.8	81.5	69.0	284.3	99.7	297.3	306.0	106.8	300.8
3	EXT	61.3	82.5	124.6	59.7	40.2	78.9	73.1	44.0	89.9	83.5	325.3	111.2	403.7	384.4	126.7	575.8
	EXTLoad	59.0	76.9	161.7	58.6	27.9	67.3	67.8	46.0	74.5	72.3	352.8	101.9	404.5	350.6	139.9	628.2
	FLEX	62.7	64.8	153.6	62.6	41.1	57.4	78.3	40.3	73.1	98.7	392.2	145.1	401.0	370.4	125.4	541.4
4	EXT	55.2	66.4	100.1	59.4	34.2	65.8	73.5	42.3	85.7	69.3	274.6	138.1	350.3	423.8	145.2	527.8
	EXTLoad	54.2	84.2	98.5	58.3	40.6	75.5	77.6	44.1	81.8	76.7	380.6	81.3	406.5	267.7	150.5	628.2
	FLEX	56.6	48.9	102.3	55.7	47.3	67.6	82.9	39.1	83.3	81.4	337.5	172.4	350.1	347.7	133.6	373.3
5	EXT	52.2	73.9	89.2	46.6	20.9	55.3	84.1	46.5	68.5	76.8	239.6	95.4	394.8	343.9	148.8	504.7
	EXTLoad	49.6	84.0	82.2	52.2	31.4	59.8	78.0	51.4	71.4	61.6	231.3	110.1	399.5	299.1	146.2	472.8
	FLEX	51.8	64.8	98.0	56.8	40.6	54.2	75.7	47.0	83.8	75.9	288.0	137.0	379.4	352.3	136.4	400.1
6	EXT	49.7	80.7	138.1	56.8	31.2	64.7	80.1	42.1	75.2	80.8	335.5	108.6	389.5	307.0	150.0	516.4
	EXTLoad	54.4	69.7	139.7	56.7	32.7	73.7	85.9	40.5	73.4	81.0	279.2	98.1	374.8	365.4	150.2	527.0
	FLEX	47.7	59.7	135.1	58.1	38.0	68.2	87.2	44.2	83.9	86.2	341.7	123.3	356.9	329.8	142.4	459.8

Table 6: Results of linear mixed models comparing the three treatments (EXT, EXTLoad, FLEX) with treatment as a fixed effect and horse as a random effect. Significant treatment effects are indicated in bold (P <0.05). CSA=cross-sectional area.

Structure	Measurement	P value
Cranial cruciate ligament	Length	0.77
	CSA	0.65
	Tibial angle	**<0.001**
Caudal cruciate ligament	Length	0.96
	CSA	0.08
	Tibial angle	**<0.001**
Medial collateral ligament	Length	**0.04**
	CSA	0.43
Lateral collateral ligament	Length	0.84
	CSA	**0.009**
Medial meniscus	Cranial horn CSA	**0.03**
	Midbody CSA	**0.002**
	Caudal horn CSA	**0.004**
Lateral meniscus	Cranial horn CSA	0.10
	Midbody CSA	**<0.001**
	Caudal horn CSA	**<0.001**

Table 7: Results (P values) of pairwise comparisons between treatments (EXT, EXTLoad, and FLEX) for measurements which had significant treatment effects identified on the linear mixed model. Significant differences between conditions are indicated in bold (P <0.05). CSA=cross-sectional area.

		FLEX-EXT	EXTLoad-EXT	EXTLoad-FLEX
Cranial cruciate ligament	Tibial angle	**<0.001**	0.63	**<0.001**
Caudal cruciate ligament	Tibial angle	**0.002**	0.63	**0.003**
Medial collateral	Length	0.11	0.53	**0.04**
Lateral collateral	CSA	**0.04**	0.64	**0.02**
Medial meniscus	Cranial horn CSA	**0.03**	0.54	0.09
	Midbody CSA	**0.02**	0.48	**0.01**
	Caudal horn CSA	0.05	0.32	**0.01**
Lateral meniscus	Midbody CSA	**0.02**	0.06	**<0.001**
	Caudal horn CSA	**0.002**	0.78	**0.001**